Responsive Multi-Domain Free-Standing Films of Gold Nanoparticles Assembled by DNA-Directed Layer-by-Layer Approach.

ARTICLE *in* NANO LETTERS · AUGUST 2013

Impact Factor: 13.59 · DOI: 10.1021/nl4023308 · Source: PubMed

5 AUTHORS, INCLUDING:

Zhaoxia Qian
University of Washington Seattle
10 PUBLICATIONS **81** CITATIONS

SEE PROFILE

NANO LETTERS

Letter

pubs.acs.org/NanoLett

Responsive Multidomain Free-Standing Films of Gold Nanoparticles Assembled by DNA-Directed Layer-by-Layer Approach

Zaki G. Estephan,[†,‡] Zhaoxia Qian,[‡] Daeyeon Lee,[†] John C. Crocker,*[,†] and So-Jung Park*[,‡,§]

[†]Department of Chemical and Biomolecular Engineering and [‡]Department of Chemistry, University of Pennsylvania, Philadelphia, Pennsylvania 19104, United States

[§]Department of Chemistry and Nano Science, Global Top 5 Program, Ewha Womans University, Seoul, 120-750, Korea

S *Supporting Information*

ABSTRACT: Responsive free-standing films of gold nanoparticles are fabricated by a new approach combining the programmable DNA-directed self-assembly and the layer-by-layer (LbL) thin film fabrication technique. This approach allows for the assembly of multidomain nanoparticle films with each domain possessing distinct properties in response to external stimuli, which is essential for the formation of dynamic nanostructures. Large area free-standing films of DNA-modified gold particles are fabricated by the selective melting of a sacrificial nanoparticle domain, taking advantage of the unique sharp melting transition of DNA-modified gold nanoparticles. Furthermore, we show that released multidomain films can be designed to further split into multiple intact daughter films in a precisely controlled manner, demonstrating that this new approach provides a powerful means to fabricate free-standing nanoparticle films that are capable of programmable transformation.

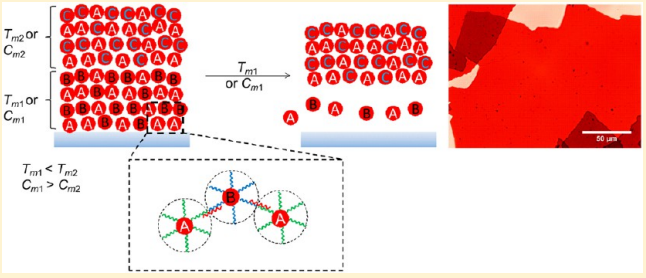

KEYWORDS: *Gold nanoparticle, DNA, layer-by-layer, free-standing film, programmable assembly, responsive material*

Since the introduction of DNA-directed self-assembly of nanoparticles in mid-1990s,[1,2] there has been tremendous effort and interest in utilizing the concept in various applications ranging from materials syntheses to bioanalysis and medicine.[3−7] DNA-modified nanoparticles have been used as a building block to form macroscopic nanoparticle aggregates, ordered superlattices,[8−13] and small clusters with a controlled coordination number[14] through the sequence specific interaction of DNA. A number of studies have shown that the structural parameters of DNA-linked nanoparticle assemblies can be readily controlled by varying the length and sequence of DNA strands and other self-assembly conditions.[9,11,15,16] In addition to three-dimensional structures, the DNA-directed assembly has been used to form mono- or multilayer films of gold nanoparticles on glass slides,[17] which formed the basis for many chip-based DNA detection methods.[5] In a different approach, Luo and co-workers reported the formation of free-standing monolayer films of DNA-modified gold nanoparticles by a drying process, where DNA was used as a simple steric barrier.[18,19]

Despite the extensive research in this area, the programmability afforded by the sequence specific DNA interactions has not been utilized for the fabrication of multidomain nanoparticle arrays with distinct domain composition and properties integrated into a single entity, which is the key step toward the fabrication of dynamic nanostructures such as actuators, motors, and robotics. Rather, most previous studies have been focused on the serial production of different nanoparticle assemblies with varying structure parameters. Here, we envision that using the large library of possible DNA sequences, one can place different functionalities in desired locations of a single multidomain nanoparticle assembly, where each domain responds differently to various external stimuli. Achieving such an ambitious goal, however, is challenging because undesired cross-linking can occur among multiple components. In addition, the aggregation number (i.e., the size of assemblies) is difficult to control in typical solution phase assemblies.

To overcome these limitations, here we combined the DNA-mediated self-assembly of nanoparticles with the layer-by-layer (LbL) deposition method that allows for the fine control of thin film architecture.[20] In this approach, DNA-modified gold nanoparticles were used as a building block for LbL assembly to fabricate multidomain nanoparticle films with programmable and distinct domain properties (Scheme 1). Large area free-standing films of gold particles were successfully fabricated from the LbL film by selectively melting a sacrificial nanoparticle domain, taking advantage of the unique sharp melting transition of DNA-modified gold nanoparticles. Furthermore, we designed and fabricated free-standing nanoparticle films that split into multiple intact daughter films in response to the changes in temperature and ionic strength in a

Received: June 26, 2013
Revised: August 8, 2013

   dx.doi.org/10.1021/nl4023308 | *Nano Lett.* XXXX, XXX, XXX−XXX

Scheme 1. Description of the DNA-Mediated LbL Deposition of Gold Nanoparticles and the Fabrication of Free-Standing Films of AC by the Selective Melting of the Sacrificial Domain of AB[a]

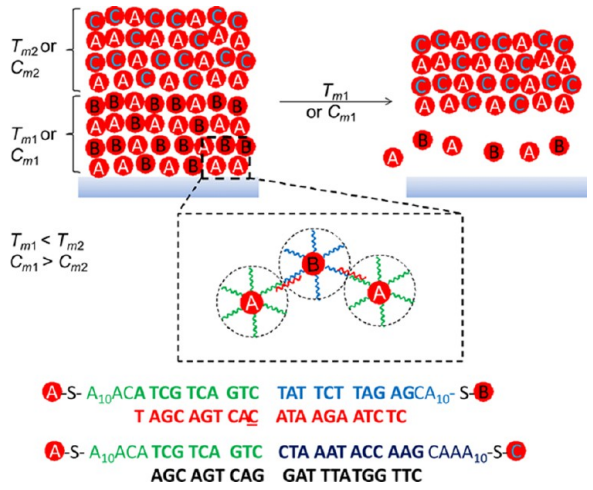

[a]The drawing does not imply any ordering in the nanoparticle film.

precisely controlled manner, demonstrating that this new approach provides a powerful tool to create dynamic, transformable nanostructures.

For DNA-mediated LbL assembly, we used a three DNA strand system composed of two different sets of gold nanoparticles (12.4 ± 1.4 nm) functionalized with thiolated oligonucleotides that are not complementary to each other and a linker DNA that connects the two sets of nanoparticles by duplex formation (Scheme 1). To fabricate a nanoparticle film composed of two distinct layered domains (Scheme 1), gold nanoparticles were functionalized with three different DNA sequences (sequences, **1**, **2**, **3**,) to produce three types of particles which are termed **A**, **B**, and **C**, respectively (Scheme 1 and Table 1). The DNA sequences were designed in such a way that type **A** particles hybridize with type **B** or type **C** particles in the presence of linkers **P** or **Q**, respectively. A single base mismatch was introduced in the **1**-**P** DNA duplex forming the **AB** domain (Scheme 1, underlined) in order to lower its melting temperature (T_m) sufficiently from that of the **AC** domain, which provided an ample temperature window to manipulate **AB** and **AC** domains independently.

In building such multidomain films, DNA sequences and LbL conditions should be carefully designed to avoid the replacement of DNA linkers in the prebuilt domain by the newly introduced DNA linkers in solution, because this sequence exchange can lead to a single domain film rather than the desired multidomain film (see Supporting Information for details). For example, we initially attempted to build a two-domain film by varying only the length of linker DNA strands. In that design, the first domain was constructed by connecting the particle **A** and **C** with a short linker **Q**, and the second domain was built by connecting the same particles with a longer linker **Q*** (Table 1), expecting that the first and the second domain would melt at 51.9 ± 0.2 and 62.1 ± 0.1 °C, respectively. However, the exposure of an **AC** film prepared with the linker **Q** to a solution containing **Q*** resulted in an exchange between the two linkers, which led to a single domain film linked with **Q*** melting at 63.0 ± 1.2 °C (Figure S1 in Supporting Information). Therefore, both thermodynamic and kinetic factors should be considered in fabricating multidomain DNA-linked LbL films of nanoparticles. In the design presented in Scheme 1, the linker exchange was avoided by adopting three different particles. The thermodynamic consideration and the strand exchange becomes more important when building more complex architecture (vide infra).

Typically, nanoparticle films were built on a glass substrate by repeated alternate exposure of the substrate to **A** and **B** (or **A** and **C**) nanoparticle solutions (10 nM) prehybridized with the corresponding linkers in 0.3 M phosphate buffered saline (PBS, 0.3 M NaCl, 10 mM phosphate buffer, pH 7.0). The glass substrate was functionalized with 3-aminopropyltrimethoxysilane to deposit the first monolayer of nanoparticles by the electrostatic interaction between the negatively charged particles and the positively charged glass substrate. On the basis of kinetic measurements (Supporting Information, Figure S2), the deposition time for each layer was set to 30 min to ensure enough nanoparticle deposition per each dipping and to avoid severe asymmetric build-up. Here, "a layer" is defined as nanoparticles accumulated by one dipping step in **A**, **B**, or **C** solution, and a "bilayer" is defined as nanoparticles accumulated by the two consecutive dipping steps in **A** and **B** or **A** and **C**. The terminology $(\mathbf{AB})_x(\mathbf{AC})_y$ is used to describe the film composition where x is the bilayer number of **AB** film and y is the bilayer number of **AC** film. The extinction increase at 530 nm with the repeated alternate dipping of the substrate into the **A** and **C** (or **A** and **B**) solutions indicates the build-up of nanoparticles on the substrate (Figure 1a). Figure 1b presents nanoparticle deposition profiles for single domain films of $(\mathbf{AB})_6$ and $(\mathbf{AC})_6$ and a two-domain film of $(\mathbf{AB})_3(\mathbf{AC})_3$. The quicker build-up of **AC** film compared to **AB** film is due to the higher binding constant of DNA composing the **AC** film than that of the **AB** film containing a base mismatch and a less GC

Table 1. DNA Sequences Used for the Functionalization and Hybridization of Au Nanoparticles

Designation	Sequence	Comments
1	5' M_1A_{10} ACA TCG TCA GTC 3'	Type **A** particle
2	5' TAT TCT TAG AGC $A_{10}M_2$ 3'	Type **B** particle
3	5' CTA AAT ACC AAG CAA $A_{10}M_2$ 3'	Type **C** particle
Linker P	5' CTC TAA GAA TA CAC TGA CGA T 3'	Hybridizes to 1 and 2, (TT)†
Linker Q	5' CTT GGT ATT TAG GAC TGA CGA 3'	Hybridizes to 1 and 3, (TT)†
Linker Q*	5' TTG CTT GGT ATT TAG GAC TGA CGA TGT 3'	Hybridizes to 1 and 3, (TT)† (Longer version of **Q**)
Linker Q^o	5' T GGT ATT TAG GAC TGA CGA 3'	Hybridizes to 1 and 3, (TT)† (Shorter version of **Q**)
Linker R	5' TT GGT ATT TAC GCT CTA AGA 3'	Hybridizes to 2 and 3, (HT)†

Underlined base represents a mismatch. See Supporting Information for M_1 and M_2 modification codes. †(TT) corresponds to tail-to-tail interaction and (HT) corresponds to head-to-tail interaction.

dx.doi.org/10.1021/nl4023308 | *Nano Lett.* XXXX, XXX, XXX−XXX

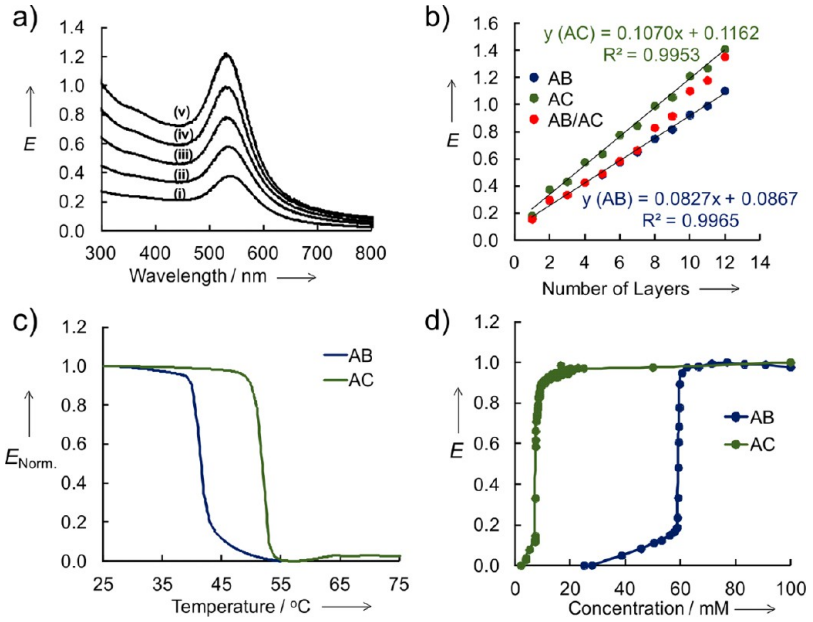

Figure 1. (a) UV−vis spectra of (i) 1, (ii) 2, (iii) 3, (iv) 4, and (v) 5 bilayers of **AC** showing the increase in the surface plasmon resonance peak at 530 nm. (b) Nanoparticle deposition profile for $(\mathbf{AB})_6$ (blue circle), $(\mathbf{AC})_6$ (green circle), and $(\mathbf{AB})_3/(\mathbf{AC})_3$ film (red circle) measured at every dipping step using the dipping time of 30 min. (c) Temperature-induced melting profiles and (d) salt-induced melting profiles for $(\mathbf{AB})_6$ and $(\mathbf{AC})_6$. All deposition and melting profiles were constructed by measuring the extinction at 530 nm.

content. Switching from the **AB** to the **AC** pair was accompanied by the expected slope change (Figure 1b, red), indicating a successful formation of an **AC** domain on top of the **AB** domain.

The melting profiles of single domain films of **AB** and **AC** were obtained (Figure 1c,d and Supporting Information, Figure S3 and S4) by following the extinction at 530 nm while increasing the temperature or decreasing the salt concentration. Both temperature- and salt-induced melting profiles showed sharp melting transitions as expected for DNA-linked nanoparticle assemblies.[21−23] As shown in Figure 1c, $(\mathbf{AB})_6$ and $(\mathbf{AC})_6$ melted at 41.6 ± 1.1 and 51.9 ± 0.2 °C with fwhm of 2.3 ± 0.1 and 2.5 ± 0.1 °C, respectively, which provided a wide 10 °C window to induce selective melting of the **AB** domain without the dissociation of the **AC** domain. Similarly, the melting salt concentration (C_m) of **AB** and **AC** films differ significantly with 59.2 ± 0.8 mM for $(\mathbf{AB})_6$ and 7.8 ± 0.9 mM for $(\mathbf{AC})_6$, giving a sufficient concentration window for the selective **AB** melting (Figure 1d). Note that the salt-induced melting is extremely sharp as reflected by the very narrow fwhm (Supporting Information, Figure S4), suggesting that many sets of different nanoparticle domains can be built into a thin film and independently manipulated by varying the ionic strength.

Taking advantage of the unique sharp melting transition of DNA-linked nanoparticles, we fabricated free-standing nanoparticle films by the selective melting of a sacrificial domain. Typically, a two domain film of $(\mathbf{AB})_x(\mathbf{AC})_y$ was built with $(\mathbf{AB})_2$ as the sacrificial region as shown in Scheme 1. Three different films of $(\mathbf{AB})_2(\mathbf{AC})_5$, $(\mathbf{AB})_2(\mathbf{AC})_{10}$, and $(\mathbf{AB})_2(\mathbf{AC})_{15}$ were prepared to release free-standing films of **AC** with varying film thicknesses. The selective melting of **AB** domain was carried out by placing the LbL films in 0.3 M PBS solution, followed by increasing the temperature to 45 °C which is above the melting temperature of the **AB** domain and below the melting temperature of the **AC** domain. Alternatively, release attempts were made by placing the film into 50 mM PBS buffer, which is below the melting salt concentration of **AB** and above that of **AC**. Note that the same DNA sequences without nanoparticles show relatively broad fwhm of 10 °C, and thus one sequence cannot be independently dissociated without affecting the other.

The selective melting of **AB** and release of **AC** free-standing films was successful in both thermal- and salt-gradient melting. A facile release was observed with a gentle shaking, and the release process was complete in ca. 2 min. Figure 2a shows a photograph of an LbL film before and after the release (i and iii). The optical microscope images of the released **AC** films are presented in Figure 2b−e, which revealed large area films of nanoparticles in the size range over hundreds of micrometers. Note that other elegant examples of solution phase formation of free-standing nanoparticle films are typically in the size range of submicrometers.[24,25] In fact, most previously reported methods for the fabrication of large area nanoparticle films relied on drying processes[26−30] where it is difficult to control the film composition. The released films of $(\mathbf{AC})_5$ and $(\mathbf{AC})_{10}$ were flexible and tend to roll up into tubes (Figure 2b,c), while thicker $(\mathbf{AC})_{15}$ films were released as rigid flat films (Figure 2d,e). SEM images of the released film of $(\mathbf{AC})_{15}$ clearly show that they are composed of discrete nanoparticles (Figure 2f). They also show that the released films maintain the overall shape when they are dried (Supporting Information, Figure S5).

Optical microscope imaging of the film release process revealed that film tearing occurs at locations where the film is pinned to the glass substrate (Supporting Information, Figure S6, Movie 1). These pinned sites appear to be nanoparticles coalesced on the surface. The lateral dimension of the released film is therefore determined by the spatial distribution of these sites. The strain exerted by the different volume expansion of **AB** and **AC** domains[8,9] might also contribute to the film fragmentation and cause the rolling of the released film. During the release process, the dissolving **AB** domain is under

dx.doi.org/10.1021/nl4023308 | *Nano Lett.* XXXX, XXX, XXX−XXX

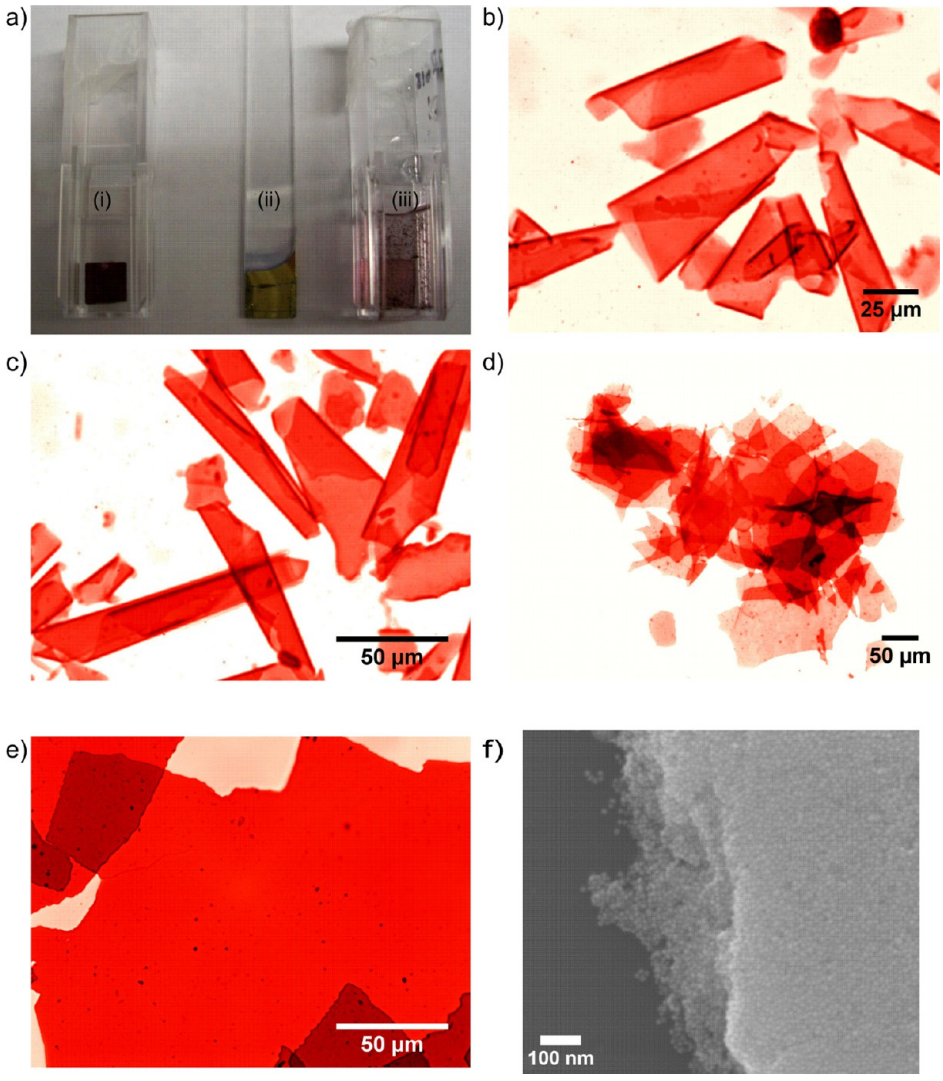

Figure 2. (a) A photograph of a glass-supported $(\mathbf{AB})_2(\mathbf{AC})_{15}$ film in 0.3 M PBS (i), a glass-supported $(\mathbf{AB})_2(\mathbf{AC})_{15}$ film taken out of PBS (ii), and free-standing $(\mathbf{AC})_{15}$ films suspended in 0.3 M PBS obtained by the selective melting of **AB** at 45 °C (iii). (b–e) Optical microscope images of released $(\mathbf{AC})_5$ (b), $(\mathbf{AC})_{10}$ (c), and $(\mathbf{AC})_{15}$ (d,e) films in 0.3 M PBS. These images are artificially colored from b/w images to reflect the colors observed by eyes. (f) An SEM image of a released film.

compressive stress while the **AC** domain is under tensile stress, which can lead to strain-induced rolling as observed in other semiconductor or polymeric systems.[31−33]

Finally, more complex four-domain films were fabricated to demonstrate the domain-selective responsive property of our free-standing nanoparticle films (Scheme 2). In this design, linker **R** was used to connect **B** and **C** particles and to build a sacrificial **BC** domain. As illustrated in Scheme 2, a $(\mathbf{BC})_3(\mathbf{AC})_5(\mathbf{AB})3(\mathbf{AC})_7$ film was first constructed on a glass slide, and then the upper three domain films of $(\mathbf{AC})_5(\mathbf{AB})_3(\mathbf{AC})_7$ were released as free-standing films by the selective dissociation of the **BC** domain.

The design and construction of four-domain films required a careful thermodynamic consideration as mentioned above (see Supporting Information for details). As shown in Figure 3, the **BC** domain with a low T_m (31.1 ± 0.1 °C, Supporting Information, Figure S7c) was found to dissociate when the film was placed in a solution containing linker **P** (Figure 3a) or **Q** (Figure 3b). The LbL assembly procedure was therefore modified to avoid the film dissolution during the LbL deposition of subsequent domains. First, a shorter linker **Q°** was used to construct the **AC** domain instead of **Q**. In addition, linker **R** was added to all subsequent LbL solutions at the **P**/**Q°**/**R** ratio of 1:1:2.5 to shift the equilibrium in favor of **BC** binding. With these modifications, desired four-domain films were successfully constructed and free-standing films of $(\mathbf{AC})_5(\mathbf{AB})_3(\mathbf{AC})_7$ were released through the selective melting of **BC** sacrificial domain by reducing the salt concentration from 0.3 to 0.15 M (Figure 4a), as illustrated in Scheme 2.

The released free-standing $(\mathbf{AC})_5(\mathbf{AB})_3(\mathbf{AC})_7$ film was designed to further split into thinner daughter films in response to ionic strength changes. Optical microscope images presented in Figure 4 and the Movie 2 (Supporting Information) revealed that a reduction of the ionic strength first induced a volume expansion of $(\mathbf{AC})_5(\mathbf{AB})_3(\mathbf{AC})_7$ films due to the increase in the electrostatic repulsion among DNA-modified nanoparticles (Figure 4b). Eventually, each $(\mathbf{AC})_5(\mathbf{AB})_3(\mathbf{AC})_7$ film was split into two intact daughter films of $(\mathbf{AC})_5$ and $(\mathbf{AC})_7$ through the dissociation and release of **A** and **B** nanoparticles in the sandwiched **AB** domain (Figure 4c and Movie 2 in Supporting Information).

dx.doi.org/10.1021/nl4023308 | *Nano Lett.* XXXX, XXX, XXX−XXX

Scheme 2. Illustration of the Build-up of a Four-Domain Film of $(BC)_m(AC)_n(AB)_x(AC)_y$ and the Release and Splitting Process of $(AC)_n(AB)_x(AC)_y$ Films

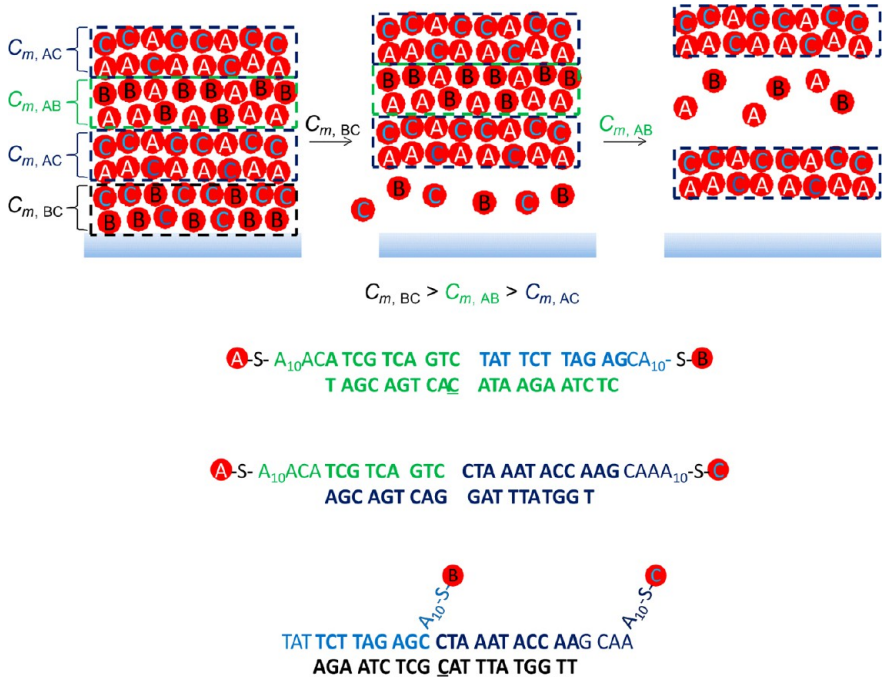

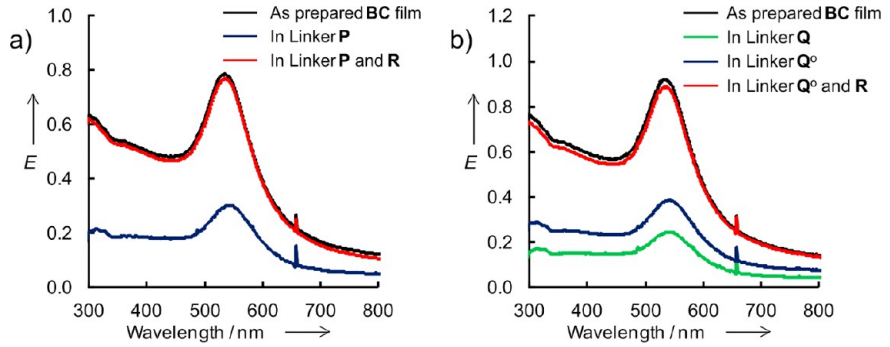

Figure 3. (a) The effect of linker **P** on the dissolution of a **BC** film built with linker **R**. The extinction at 530 nm was reduced when the film was immersed in a solution containing 0.4 μM linker **P**, indicating that the linker exchange and film dissolution occurs (blue). The film dissolution was avoided by adding linker **R** in the linker **P** solution (red). (b) The effect of linker **Q** (green) and **Q**° (blue) on the dissolution of a **BC** film built with linker **R**. To avoid the film dissolution, a shorter linker **Q**° was used instead of **Q**, and linker **R** was added in the linker **Q**° solution (red).

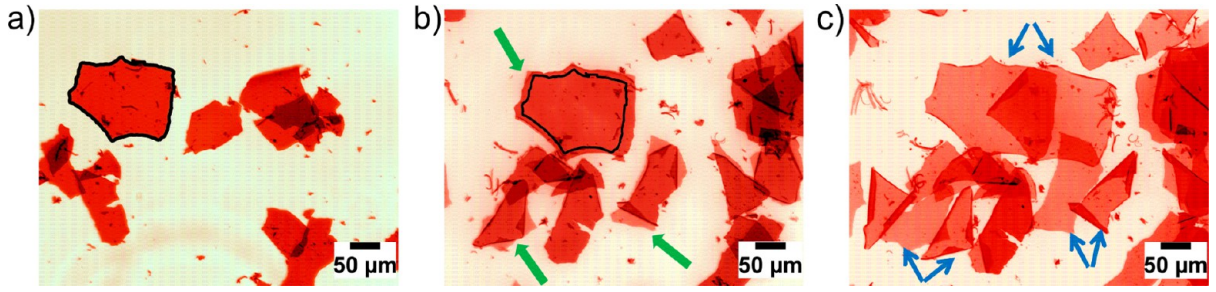

Figure 4. Optical images taken over time (a–c) showing the film splitting process. Every single film examined underwent splitting. Film expansion occurs prior to splitting as outlined by the black contour in (a) and (b). Green arrows in (b) indicate some of the $(AC)_5(AB)_3(AC)_7$ films in the progress of splitting, and blue arrows in (c) indicate split films of $(AC)_5$ and $(AC)_7$ from the $(AC)_5(AB)_3(AC)_7$ films marked by green arrows in (b). The film splitting was induced by reducing the salt concentration from 100 mM to 50 mM. See Movie 2 in Supporting Information for the complete process.

In summary, we demonstrated the fabrication of responsive free-standing nanoparticle films based on the DNA-mediated LbL assembly of nanoparticles. In this approach, the film architecture and properties are controlled by the DNA and LbL dipping sequence. The thermodynamics of the system should be carefully controlled to avoid undesired DNA exchange and

dx.doi.org/10.1021/nl4023308 | *Nano Lett.* XXXX, XXX, XXX–XXX

to produce multidomain films with predefined film architecture and distinct domain properties. Large area submillimeter sized free-standing films were successfully fabricated by the selective dissociation of the bottom sacrificial domain. While various types of responsive polymers have been employed as sacrificial layers to fabricate free-standing polymer films,[34−38] the release process using DNA-modified nanoparticles reported here offers important advantages. First, the release parameters can be tailored over wide temperature and ionic strength ranges by changing the DNA sequences used in the sacrificial layer. Second, the unique sharp melting transition of DNA-modified nanoparticles offers independent control of multiple domains. While this unique melting property of DNA-modified gold nanoparticle has been extensively exploited in developing highly sensitive and selective DNA and protein detection methods[6,39,40] it has been rarely utilized in materials assembly and fabrication. Here, we demonstrated that the sharp melting transition of densely functionalized gold nanoparticles is a valuable characteristic in DNA-based nanofabrication as well. Third, the DNA-based release required only minimal number of sacrificial layers (Supporting Information Figure S8). While two bilayers of **AB** were needed for the film release in this study, it is postulated that the release can be achieved with a single bilayer if the substrate itself was functionalized with DNA thus eliminating the electrostatic contribution to the first bilayer. On the basis of the approach, we fabricated responsive multidomain free-standing films that transform into two intact films and release free particles from the middle domain upon the reduction of ionic strength. We envision that such multidomain structures can be designed to exhibit reversible shape-shifting capabilities in response to external stimuli through the differential contraction, expansion, and melting. This capability opens up exciting possibilities for the fabrication of dynamic nanostructures such as actuators, motors, and robotics. Efforts in this direction are underway.

■ ASSOCIATED CONTENT

Supporting Information

Detailed experimental methods, free energy calculations, linker exchange experiments, kinetic experiments, and additional extinction spectra, melting profiles, and SEM images of LbL films. This material is available free of charge via the Internet at http://pubs.acs.org.

■ AUTHOR INFORMATION

Corresponding Author

*E-mail: sojungpark@ewha.ac.kr (S.-J.P); jcrocker@seas.upenn.edu (J.C.C.).

Notes

The authors declare no competing financial interest.

■ ACKNOWLEDGMENTS

This work was supported by the NSF, MRSEC seed award (DMR11-20901). S.J.P acknowledges the support from the Camille Dreyfus teacher scholar award. D.L. acknowledges support from the NSF DMR-1055594.

■ REFERENCES

(1) Mirkin, C. A.; Letsinger, R. L.; Mucic, R. C.; Storhoff, J. J. *Nature* **1996**, *382*, 607−609.
(2) Alivisatos, A. P.; Johnsson, K. P.; Peng, X. G.; Wilson, T. E.; Loweth, C. J.; Bruchez, M. P.; Schultz, P. G. *Nature* **1996**, *382*, 609−611.
(3) Kim, A. J.; Biancaniello, P. L.; Crocker, J. C. *Langmuir* **2006**, *22*, 1991−2001.
(4) Crocker, J. C. *Nature* **2008**, *451*, 528−529.
(5) Taton, T. A.; Mirkin, C. A.; Letsinger, R. L. *Science* **2000**, *289*, 1757−1760.
(6) Georganopoulou, D. G.; Chang, L.; Nam, J. M.; Thaxton, C. S.; Mufson, E. J.; Klein, W. L.; Mirkin, C. A. *Proc. Natl. Acad. Sci. U.S.A.* **2005**, *102*, 2273−2276.
(7) Rosi, N. L.; Giljohann, D. A.; Thaxton, C. S.; Lytton-Jean, A. K. R.; Han, M. S.; Mirkin, C. A. *Science* **2006**, *312*, 1027−1030.
(8) Nykypanchuk, D.; Maye, M. M.; van der Lelie, D.; Gang, O. *Nature* **2008**, *451*, 549−552.
(9) Xiong, H. M.; van der Lelie, D.; Gang, O. *J. Am. Chem. Soc.* **2008**, *130*, 2442−2443.
(10) Park, S. Y.; Lytton-Jean, A. K. R.; Lee, B.; Weigand, S.; Schatz, G. C.; Mirkin, C. A. *Nature* **2008**, *451*, 553−556.
(11) Macfarlane, R. J.; Jones, M. R.; Senesi, A. J.; Young, K. L.; Lee, B.; Wu, J. S.; Mirkin, C. A. *Angew. Chem., Int. Ed.* **2010**, *49*, 4589−4592.
(12) Casey, M. T.; Scarlett, R. T.; Rogers, W. B.; Jenkins, I.; Sinno, T.; C., C. J. *Nat. Commun.* **2012**, *3*, 1209.
(13) Noh, H.; Hung, A. M.; Cha, J. N. *Small* **2011**, *7*, 3021−3025.
(14) Fu, A. H.; Micheel, C. M.; Cha, J.; Chang, H.; Yang, H.; Alivisatos, A. P. *J. Am. Chem. Soc.* **2004**, *126*, 10832−10833.
(15) Macfarlane, R. J.; Lee, B.; Jones, M. R.; Harris, N.; Schatz, G. C.; Mirkin, C. A. *Science* **2011**, *334*, 204−208.
(16) Park, S. J.; Lazarides, A. A.; Storhoff, J. J.; Pesce, L.; Mirkin, C. A. *J. Phys. Chem. B* **2004**, *108*, 12375−12380.
(17) Taton, T. A.; Mucic, R. C.; Mirkin, C. A.; Letsinger, R. L. *J. Am. Chem. Soc.* **2000**, *122*, 6305−6306.
(18) Campolongo, M. J.; Tan, S. J.; Smilgies, D. M.; Zhao, M.; Chen, Y.; Xhangolli, I.; Cheng, W. L.; Luo, D. *ACS Nano* **2011**, *5*, 7978−7985.
(19) Tan, S. J.; Campolongo, M. J.; Luo, D.; Cheng, W. L. *Nat. Nanotechnol.* **2011**, *6*, 268−276.
(20) *Multilayer Thin Films: Sequential Assembly of Nanocomposite Materials*, 2nd ed.; Decher, G.; Schlenoff, J. B., Eds.; Wiley-VCH Verlag GmbH & Co.: Weinheim, 2012.
(21) Jin, R. C.; Wu, G. S.; Li, Z.; Mirkin, C. A.; Schatz, G. C. *J. Am. Chem. Soc.* **2003**, *125*, 1643−1654.
(22) Gibbs-Davis, J. M.; Schatz, G. C.; Nguyen, S. T. *J. Am. Chem. Soc.* **2007**, *129*, 15535−15540.
(23) Long, H.; Kudlay, A.; Schatz, G. C. *J. Phys. Chem. B* **2006**, *110*, 2918−2926.
(24) Tang, Z. Y.; Zhang, Z. L.; Wang, Y.; Glotzer, S. C.; Kotov, N. A. *Science* **2006**, *314*, 274−278.
(25) Buchkremer, A.; Linn, M. J.; Reismann, M.; Eckert, T.; Witten, K. G.; Richtering, W.; von Plessen, G.; Simon, U. *Small* **2011**, *7*, 1397−1402.
(26) Chen, Y.; Fu, J.; Ng, K. C.; Tang, Y.; Cheng, W. L. *Cryst. Growth Des.* **2011**, *11*, 4742−4746.
(27) Narayanan, S.; Wang, J.; Lin, X. M. *Phys. Rev. Lett.* **2004**, 93.
(28) Mutlugun, E.; Hernandez-Martinez, P. L.; Eroglu, C.; Coskun, Y.; Erdem, T.; Sharma, V. K.; Unal, E.; Panda, S. K.; Hickey, S. G.; Gaponik, N.; Eychmuller, A.; Demir, H. V. *Nano Lett.* **2012**, *12*, 3986−93.
(29) Ng, K. C.; Udagedara, I. B.; Rukhlenko, I. D.; Chen, Y.; Tang, Y.; Premaratne, M.; Cheng, W. L. *ACS Nano* **2012**, *6*, 925−934.
(30) Feng, D.; Lv, Y. Y.; Wu, Z. X.; Dou, Y. Q.; Han, L.; Sun, Z. K.; Xia, Y. Y.; Zheng, G. F.; Zhao, D. Y. *J. Am. Chem. Soc.* **2011**, *133*, 15148−15156.
(31) Vorob'ev, A. B.; Prinz, V. Y. *Semicond. Sci. Technol.* **2002**, *17*, 614−616.
(32) Luchnikov, V.; Sydorenko, O.; Stamm, M. *Adv. Mater.* **2005**, *17*, 1177−1182.
(33) Takahashi, M.; Figus, C.; Malfatti, L.; Tokuda, Y.; Yamamoto, K.; Yoko, T.; Kitanaga, T.; Tokudome, Y.; Innocenzi, P. *NPG Asia Mater.* **2012**, *4*, e22.
(34) Pennakalathil, J.; Hong, J. D. *Acs Nano* **2011**, *5*, 9232−9237.

(35) Zhuk, A.; Pavlukhina, S.; Sukhishvili, S. A. *Langmuir* **2009**, *25*, 14025−14029.
(36) Seo, J.; Lutkenhaus, J. L.; Kim, J.; Hammond, P. T.; Char, K. *Macromolecules* **2007**, *40*, 4028−4036.
(37) Ono, S. S.; Decher, G. *Nano Lett.* **2006**, *6*, 592−598.
(38) Dubas, S. T.; Farhat, T. R.; Schlenoff, J. B. *J. Am. Chem. Soc.* **2001**, *123*, 5368−5369.
(39) Storhoff, J. J.; Elghanian, R.; Mucic, R. C.; Mirkin, C. A.; Letsinger, R. L. *J. Am. Chem. Soc.* **1998**, *120*, 1959−1964.
(40) Chen, X. J.; Sanchez-Gaytan, B. L.; Hayik, S. E. N.; Fryd, M.; Wayland, B. B.; Park, S. J. *Small* **2010**, *6*, 2256−2260.

dx.doi.org/10.1021/nl4023308 | *Nano Lett.* XXXX, XXX, XXX−XXX